Mapping Above-ground Vegetation Biomass Using Products of Vegetation Index in a Typical Grassland

Zongyao Sha, Chunfang Wang

***Abstract*—Grassland vegetation is an important factor relating to the improvement of environment as well as a critical source of food for grassland livestock. The long-term Global Vegetation Indices (GVIs) derived from earth observation projects such as AVHRR, SPOT, and MODIS, along with other satellite data, have accumulated huge volume of dataset which could be used in applications from terrestrial vegetation monitoring to climate changes. In this paper, four GVIs, including MODIS EVI, MODIS NDVI, SPOT-VGT NDVI and AVHRR NDVI, were explored to map above-ground vegetation biomass (AG-Biomass) in the typical grassland located in the Xilingol grassland, Inner Mongolia, China. The objective was to compare the performance of inversion models (based on linear, quadratic, power and exponential functions), mapping scales (including 1 km × 1 km, 4.5 km × 4.5 km, and 8 km × 8 km), and GVIs in grassland AG-Biomass inversion, and to quantify AG-biomass distribution. On-site samples integrated with Landsat TM/ETM+ images provided satisfactory dataset for inversion evaluation. Results indicated that MODIS NDVI outperformed MODIS EVI, SPOT-VGT NDVI and AVHRR NDVI to estimate AG-Biomass. Overall, the model through a power function and the scale at 4.5 km × 4.5 km achieved the highest agreement between the on-site data and the modeled output. Considering the temporal features of the AVHRR NDVI and MODIS-NDVI, the two products were lastly adopted to map AG-Biomass at scale 8 km × 8 km over 20 years (1994-2013). This work confirmed that the freely available GVIs could be adopted to map the grassland vegetation productivity, and the spatio-temporal biomass distribution from the result showed great spatial variations.**

***Index Terms*—Biomass, Grassland, Inversion, Vegetation index,**

I. Introduction

Grasslands are important resources from both agronomic and ecological perspectives, as more than 40% of the global terrestrial landscape consists of grasslands and savannas [1,2,3]. Above-ground vegetation biomass (AG-Biomass) is one of the most important indicators that can show the health of the environment [4]. In addition, as AG-Biomass provides food for pasture animals on grassland, understanding the spatiotemporal dynamics of AG-Biomass is critical agriculture development [5]. Direct method to obtain AG-Biomass is through field surveys, which is time-consuming and expensive; therefore, AG-Biomass data acquired through field surveys are often restricted to a very narrow scope. Development of advanced geo-spatial techniques raises the possibility for acquiring vegetation biomass data in a fast and consistent way [6]. A good case is remote sensing which offers an effective means to observe the earth surface over large areas in a systematic way [7]. When coupled with field surveys, remotely sensed imagery can provide affordable and efficient way to map AG-Biomass [8].

Remotely sensed imagery that collects spectral reflectance for vegetation cover varies from spatial and temporal resolutions [9]. Various remotely sensed data has been used to map vegetation productivity at different spatial resolutions. Landsat imagery, for example, provides reflectance data at spatial scale of 30 m × 30 m and is widely applied for small scale (local or regional) land mapping [10]. On the contrary, coarse spatial resolution satellite images from AVHRR, SPOT-VGT or MODIS programs are mainly used for large scale (regional and global) mapping [11,12,13]. One commonly way to quantify AG-Biomass is through vegetation index (VI), an index computed from the combination of the reflectance bands from the imagery, and AG-Biomass can then be estimated through a technique called inversion approach [14,15]. Various VIs have been proposed to inverse AG-Biomass by series of inversion models [16]. A few concerns have been raised regarding to AG-Biomass inversion by VIs [17]. For example, due to the limited VI availability from any remote sensing imagery, identical VI value from different GVIs does not mean comparable AG-Biomass on the ground [18]. Further, due to the complicated, often nonlinear relationship between VIs and AG-Biomass, accurately inversing the latter through VIs is difficult, especially in too sparse or over dense vegetated areas.

The objective of this study was to compare the performance of different models (linear, quadratic, power and exponential functions), scales (1 km × 1 km, 4.5 km × 4.5 km, and 8 km × 8 km), and GVIs (AVHRR NDVI, SPOT-VGT NDVI, MODIS EVI and MODIS NDVI) for AG-Biomass inversion and evaluate AG-Biomass dynamics through GVIs, which can offer rapid and cost-effective ways for producing AG-Biomass series and thus provides key dataset for evaluating the environment as well as making decisions on agriculture production.

II. Methodology

A. Study Area

This work was done in the typical grassland in Xilingol, Inner Mongolia, China (Figure 1). Xilingol River Basin, situated 43°26′-44°29′N and 115°32′-117°12′E, is one of the most representative steppe zones in northern China and even in the vast semi-arid region of Eurasian continent [19,20],

Manuscript received March 16, 2017. This work was supported in part by the NSFC 41371371.

Z.Y. Sha is with Wuhan University, Wuhan, Hubei 430079 China (e-mail:zongyaosha@163.com).

C.F Wang is with Huazhong Agricultural University, Wuhan, Hubei 430079 China (e-mail:cfwang@hzau.edu.cn).

with the latter serving as one of the most important areas for food production and environmental security in the world [20,21,22]. Systematic collections of climate, soil, vegetation, and ecosystem data have been conducted since a permanent ecosystem observation station (EOB) was established in Xilingol in 1979 by the Chinese Academy of Sciences, and this has provided comprehensive support for grassland and related research activities.

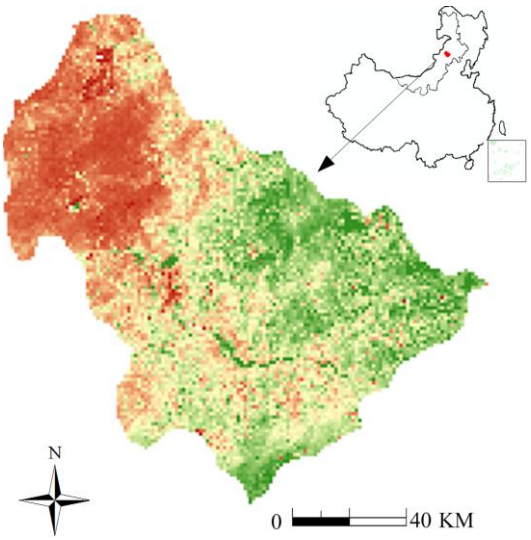

Fig. 1. Study area.

B. Data collection and analysis

Field trip conducted in August, 2004 collected 461 AG-Biomass ground samples. Artificial Neutral Network (ANN) was employed to map AG-Biomass distribution using the spectral reflectance bands from two concurrent Landsat ETM+/TM scenes (at scale 30 m × 30 m). Readers interested in detail information about the data collection and AG-Biomass mapping using ANN through Landsat ETM+/TM imagery can refer to our previous work [23]. Four freely available GVIs, namely, AVHRR NDVI, SPOT-VGT NDVI, MODIS EVI and MODIS NDVI, were acquired and used to evaluate their performance in inversing AG-Biomass. The availability of AVHRR NDVI from Global Inventory Modeling and Mapping Studies (GIMMS) strides from 1981 to 2006; SPOT-VGT NDVI is available from 1998 to the present; MODIS NDVI/EVI data is available from 2000 to the present. Since MODIS EVI/NDVI (MOD13A2, 16-day synthesis based on maximum value composite) and SOPT-VGT NDVI (10-day synthesis, S10) are both at scale 1 km × 1 km whereas GIMMS AVHRR NDVI is provided at scale 8 km × 8 km, three mapping scales, i.e., 1 km × 1 km, 4.5 km × 4.5 km, and 8 km × 8 km, were designed to examine the scale effect on AG-Biomass inversion. Specifically, in addition to the scale at 1 km × 1 km, both MODIS EVI/NDVI and SOPT-VGT NDVI were resampled to 8 km × 8 km and 4.5 km × 4.5 km (the medium level of 1 km × 1 km and 8 km × 8 km) by method of the nearest neighbor, making them comparable to AVHRR NDVI and enabled us to examine the scale effect in the AG-Biomass inversion. The field sampling plots and those coarse GVIs are not scale-compatible; directly using field collected data to validate the modeling results was void. Therefore, the AG-Biomass map (30 m × 30 m) from the Landsat ETM+/TM was resampled to the same scales (1 km × 1 km, 4.5 km × 4.5 km, and 8 km × 8 km), offering "real" AG-Biomass data or ground truth samples to evaluate GVIs in the AG-Biomass inversion. A simple pixel-averaging strategy was employed to downscale products (GVI and AG-Biomass map) from the finer resolution data [13]. The models of inversing AG-Biomass by remote sensing technique vary from simple linear regressions to more advanced machine learning algorithms (e.g., artificial neutral network or support vector machine); some of the models require additional input variables rather than VI alone [23,24,25]. Here easy-to-apply ones simply using VI as input were tested, considering that it might be difficult to obtain additional variables especially when historical AG-Biomass mapping is desired [26]. Based on an exploratory analysis of bivariate scatter plots (AG-Biomass vs. GVIs), four models, i.e., linear, quadratic, power, and exponential functions (VI as independent variable and AG-Biomass as dependent) were selected with formula expressed as Eq. (1) ~ (4), respectively,

$$AG\text{-}Biomass_i = a + b*VI_i \quad (1)$$

$$AG\text{-}Biomass_i = a + b*VI_i + c*VI_i^2 \quad (2)$$

$$AG\text{-}Biomass_i = a*VI_i^b \quad (3)$$

$$AG\text{-}Biomass_i = a*e^{b*VI_i} \quad (4)$$

where i represents the year examined, AG-Biomass is the aboveground biomass in the peak growing season of year i, VIi is the value of vegetation index from each GVIs for the corresponding AG-Biomassi, and a, b, and c are the coefficients to be fit. Those functions have been applied extensively in similar work and proved to be simple and easy to use [27,28]. In the current study, two thirds of the 461 ground samples (n=310) were used to fit the models while the rest (n=151) were used for evaluation purpose.

C. Result evaluation

The performance of the GVIs at the three mapping scales by each of the models was compared based on two criteria: 1) coefficient of determination (R^2) of each model, and 2) the generality agreement between modeled values vs. ground samples. The use of R^2 is to test the goodness of fit for a model by the following equation,

$$R^2 = 1 - \frac{\sum_i^n (y_i - \hat{y}_i)^2}{\sum_i^n (y_i - \bar{y})^2} \quad (5)$$

where $\hat{y}_i$ is the modeled value, y_i is the "real" value, $\bar{y}$ is the mean value of y_i (i=1, 2, …, 310). R^2 provides a measure of how well observed outcomes are replicated by each model. The generality agreement was based on the modeled values and the ground truth data from the testing samples. This agreements were evaluated by RMSE (total root–mean–square errors) and $RMSE_r$ (relative RMSE), which were defined as follows [29].

$$\mathrm{RMSE} = \sqrt{\frac{1}{n}\sum_{i=1}^{n}(y_i - \hat{y}_i)^2} \quad (6)$$

$$\mathrm{RMSE}_r = \frac{\sqrt{\frac{1}{n}\sum_{i=1}^{n}(y_i - \hat{y}_i)^2}}{\bar{y}} \times 100 \quad (7)$$

where $\hat{y}_i$ is the modeled value, y_i is the "real" value, $\bar{y}$ is the mean of y_i (i=1, 2, …, 151).

III. RESULTS

A. Comparison of AG-Biomass Inversion

A AG-Biomass map was built on the field samples and the concurrent Landsat images using ANN models. Reasonable accuracy (RMSEr from 39.88% to 53.20%) was achieved and the map was used to extract "real data" to fit each model and to test the performance of AG-Biomass inversion from the GVIs. The resampled AG-Biomass maps at the three scales are shown in Figure 2. Those maps expressed an identical distribution trend of AG-Biomass which decreased from the south-east to the north-west. When the AG-Biomass maps at each scale are compared to the GVIs (e.g., GVI maps at 1 km × 1 km in Figure 3 and at 8 km × 8 km in Figure 4), they seem to present similar changing mode.

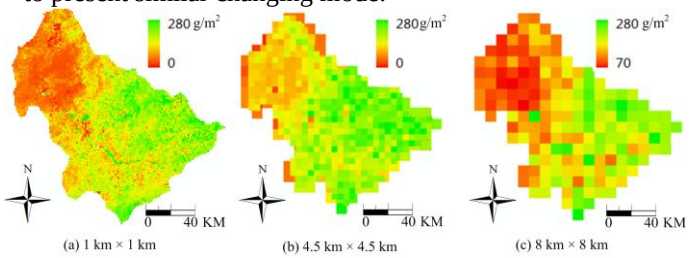

Fig. 2. AG-Biomass resampled to resolutions at (a)1 km × 1 km, (b)4.5 km × 4.5 and (c) 8 km × 8 km

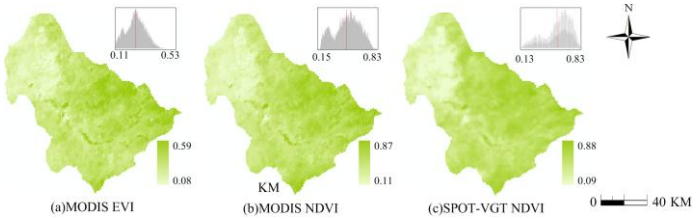

Fig. 3. VI distributions and their histograms at scale 1 km ×1 km

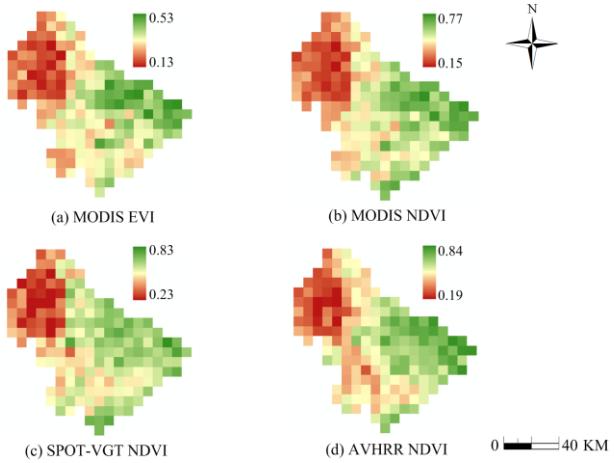

Fig. 4. VI distributions at scale 8 km ×8 km

Table 1 compares the fitting result (functions and their R^2) between the AG-Biomass and the GVIs by different inversion models. All the GVIs could be used to map AG-Biomass distribution through the models (all were significant at $p<0.01$). The coefficient of determination (R^2) was evaluated from three aspects: mapping scale, inversion function, and GVIs. From the perspective of mapping scale, the resolution at 4.5 km × 4.5 km showed the best fit, as indicated by the highest R^2. The resolution at 8 km × 8 km showed the lowest agreement while the performance at 1 km × 1 km was at medium level. Furthermore, the performance varied among GVIs and spatial resolutions from the aspect of model functions. The best inversion one for MODIS VIs (both EVI and NDVI) were the power function at all the scales. However, the performance from SPOT-VGT NDVI was closely related to the scales: exponential function showed consistently better fit at scales of both 1 km × 1 km and 4.5 km × 4.5 km (R^2=0.657) while the power function presented best performance at the scale 8 km × 8 km (R^2=0.544). AVHRR NDVI presented similar result to MODIS VIs, i.e., power function demonstrated the highest consistency at scale 8 km × 8 km (R^2=0.515). In summary, the power function achieved consistently better performance at scale 8 km × 8 km for all the GVIs. Among GVIs, the best was MODIS NDVI which had consistently highest R^2 by all the models at all scales, followed by MODIS EVI, SPOT-VGT-NDVI and AVHRR NDVI, though the latter only included a single scale (8 km × 8 km).

The total root-mean-square errors (RMSE) and the relative RMSE (RMSEr) were further compared after the fit models were applied on the testing samples (Table 2). RMSE was valued within 20~40 g/m^2 while all the RMSEr were under 20%, proving that all the models resulted in only a limited error. The performance of the models from the RMSE and RMSEr were generally consistent with that evaluated from the R^2 values in the model fitting.

B. AG-Biomass Dynamics from GVIs

Significant temporal differences indicated by the standard deviation (std) of AG-Biomass over the 20 years were observed. There are 5 categories in terms of the temporal AG-Biomass trajectory pattern, including extremely substantial reduction (ESR), substantial reduction (SR), non-substantial (NS), substantial increase (SI) and extremely substantial increase (ESI). The significance analysis revealed spatial distribution of those changing patterns. Areas with substantially increased vegetation NPP trend (including SI and ESI, totaled about 18% of the area) were found to be mainly distributed in the central part. Nearly one third of the study area (34%) which were located primarily in the western and southern part showed non-substantial changing pattern in NPP. About half of the study area, including most part of the north-eastern area as well as part of the southern area in the central part, showed substantial decreased NPP trend indicating severe grassland ecosystem deterioration.

IV. DISCUSSION AND CONCLUSION

The GVIs have been applied to investigate long-term vegetation productivity (AG-Biomass). Though there are some advanced approaches to derive other forms of vegetation index from remotely sensed imagery, publicly available VI time series (e.g., MODIS EVI, MODIS NDVI, SPOT-VGT NDVI and AVNHRR NDVI) have provided convenient proxy for cost-effective AG-Biomass mapping at regional or global scale [26]. To make informed decision on the selection of GVIs, one needs to understand the pros and cons of each product since the VIs may demonstrate different characteristics under different contexts of mapping purposes

[18]. The study revealed that the most suitable VIs for mapping AG-Biomass in the grassland was MODIS NDVI. It is known that the remotely sensed imagery from MODIS contains more spectral information and MODIS EVI/NDVI are produced through more advanced data preprocessing techniques as compared to the counterparts like SPOT-VGT NDVI and AVHRR NDVI [28,30]. The advantage of MODIS VIs was confirmed in this study, as they (both MODIS NDVI and EVI) showed more promising result compared to SPOT-VGT NDVI and AVHRR NDVI. MODIS EVI is usually believed to be an improved version of NDVI and has been used for estimating AG-Biomass such as forestry [31]. Interestingly, the study showed that MODIS NDVI had better performance than MODIS EVI. This finding seems to be consistent with the previous study, which showed that AG-Biomass had better correlation to vegetation index NDVI than EVI in grassland area [32]. Nevertheless, MODIS EVI was designed to overcome the background effect and greenness saturation of vegetation, it showed a more compressed and narrower histogram (from 0.08 to 0.59) than that of MODIS NDVI (from 0.11 to 0.87) (Figure 3). This narrower distribution might make MODIS EVI less sensitive in response to the AG-Biomass changes than MODIS NDVI. This assumption might be reasonable considering that the mapped AG-Biomass was concurrent to the growing peak of the grassland vegetation which exhibited moderate cover density (neither too sparse to avoid background effect, nor too dense to be affected by greenness saturation).

The mapping scale is another consideration in AG-Biomass inversion through remote sensing datasets [33]. Different performances were observed at the three scales (i.e., 1 km × 1 km, 4.5 km × 4.5 km and 8 km × 8 km). Neither scale at 1 km × 1 km nor scale at 8 km × 8 km achieved the highest mapping consistency; instead, the intermediate level (4.5 km × 4.5 km) demonstrated best agreement between the inversed AG-Biomass and "real data". Scale effect on AG-Biomass inversion is complicated. Small scale VIs from remotely sensed imagery could bring detail information about grassland ecosystem but they might be too sensitive to noisy data; conversely, large scale mapping through spatial averaging has the advantage of minimizing local anomalies but may smooth out important spatial heterogeneity of mapping features[13,34]. This study found that mapping scale at 4.5 km × 4.5 km could bring the best result. Thought only limited scale levels were tested, it does suggest that an appropriate intermediate mapping scale located within the range of 1 km × 1 km and 8 km × 8 km might be used for better AG-Biomass inversion from GVIs for the grassland.

In summary, AG-Biomass, as an indicator for vegetation productivity, provides key insight for understanding the impact on the environment from grassland. However, to obtain reliable AG-Biomass data from remotely sensing imagery through inversion approach, a few considerations should be made. This work showed that all the publically available GVIs could be used to inverse AG-Biomass. In terms of the selection of the VI datasets, MODIS NDVI proves to be the superiority followed by MODIS EVI. The scales at 1 km × 1 km, 4.5 km × 4.5 km and 8 km × 8 km can all be used to inverse the AG-Biomass distribution in the study region. The smallest scale, namely 1 km × 1 km did not produce the best result and the most suitable mapping scale was located between 1 km × 1 km and 8 km × 8 km. The inversion model with a power function showed the best result. We used AVHRR NDVI and MODIS-NDVI to make long-term AG-Biomass which showed great spatio-temporal variations. Overall, the work demonstrates that a promising outcome to map the long-term AG-Biomass in the grassland could be achieved by applying the optimal inversion model at the suitable mapping scale simply with data input from the GVIs and the combination of GVIs could provide acceptable data sources for estimating vegetation biomass which is the main food for the grassland livestock.

REFERENCES

(Periodical style)

[1] Moore, C. Distribution of grasslands. In *Grasses and Grasslands*; Barnard, C., Ed.; Macmillan: New York, USA, 1966; pp. 182–205.

[2] Chapin, F. S.; Sala, O.; Huber-Sannwald, E. *Global biodiversity in a changing environment: Scenarios for the 21st century*; Springer: New York, USA, 2001; pp. 121-137.

[3] Yu, L.; Zhou, L.; Liu, W.; Zhou, H. Using Remote Sensing and GIS Technologies to Estimate Grass Yield and Livestock Carrying Capacity of Alpine Grasslands in Golog Prefecture, China. Pedosphere, vol. 20, no. 3, pp. 342-351. May 2010.

[4] Zhao, F.; Xu, B.; Yang, X.; Jin, Y.; Li, J.; Xia, L. Remote Sensing Estimates of Grassland Aboveground Biomass Based on MODIS Net Primary Productivity (NPP): A Case Study in the Xilingol Grassland of Northern China. Remote Sensing 2014, 6(6), 5368-5386.

[5] Edirisinghe, A.; Clark, D.; Waugh, D. Spatio-temporal modelling of biomass of intensively grazed perennial dairy pastures using multispectral remote sensing. International Journal of Applied Earth Observation and Geoinformation 2012, 16, 5-16.

[6] Gao, J. Quantification of grassland properties: How it can benefit from geoinformatic technologies? International Journal of Remote Sensing 2006, 27(7), 1351-1365.

[7] Wasige, J. E.; Groen, T. A.; Smaling, E.; Jetten, V. Monitoring basin-scale land cover changes in Kagera Basin of Lake Victoria using ancillary data and remote sensing. International Journal of Applied Earth Observation and Geoinformation 2013, 21, 32-42.

[8] Ahamed, T.; Tian, L.; Zhang, Y.; Ting, K. A review of remote sensing methods for biomass feedstock production. Biomass and Bioenergy 2011, 35(7), 2455-2469.

[9] Ming, D.; Yang, J.; Li, L.; Song, Z. Modified ALV for selecting the optimal spatial resolution and its scale effect on image classification accuracy. Mathematical and Computer Modelling 2011, 54(3-4), 1061-1068.

[10] Yang, J.; Weisberg, P. J.; Bristow, N. A. Landsat remote sensing approaches for monitoring long-term tree cover dynamics in semi-arid woodlands: Comparison of vegetation indices and spectral mixture analysis. Remote Sensing of Environment 2012, 119, 62-71.

[11] Fensholt, R.; Proud, S. R. Evaluation of Earth Observation based global long term vegetation trends — Comparing GIMMS and MODIS global NDVI time series. Remote Sensing of Environment 2012, 119, 131-147.

[12] Caccamo, G.; Chisholm, L.; Bradstock, R.; Puotinen, M. Assessing the sensitivity of MODIS to monitor drought in high biomass ecosystems. Remote Sensing of Environment 2011, 115(10), 2626-2639.

[13] Tarnavsky, E.; Garrigues, S.; Brown, M. E. Multiscale geostatistical analysis of AVHRR, SPOT-VGT, and MODIS global NDVI products. Remote Sensing of Environment 2008, 112(2), 535-549.

[14] Hong, S.; Shin, I. A physically-based inversion algorithm for retrieving soil moisture in passive microwave remote sensing. Journal of Hydrology2011, 405(1-2), 24-30.

[15] Ullah, S.; Si, Y.; Schlerf, M.; Skidmore, A. K.; Shafique, M.; Iqbal, I. Estimation of grassland biomass and nitrogen using MERIS data. International Journal of Applied Earth Observation and Geoinformation 2012, 19, 196-204.

[16] Muñoz, J. D.; Finley, A. O.; Gehl, R.; Kravchenko, S. Nonlinear hierarchical models for predicting cover crop biomass using Normalized Difference Vegetation Index. Remote Sensing of Environment 2010, 114(12), 2833-2840.

[17] Jia, W.; Liu, M.; Yang, Y.; He, H.; Zhu, X. Estimation and uncertainty analyses of grassland biomass in Northern China: Comparison of multiple remote sensing data sources and modeling approaches. Ecological Indicators 2016, 60, 1031-1040.

[18] Fensholt, R.; Rasmussen, K.; Nielsen, T. T.; Mbow, C. Evaluation of earth observation based long term vegetation trends — Intercomparing NDVI time series trend analysis consistency of Sahel from AVHRR GIMMS, Terra MODIS and SPOT VGT data. Remote Sensing of Environmen 2009, 113(9), 1886-1898.
[19] Li, B.; Yon, S.P.; Li, Z.H. Vegetation and Its Utilization in Xilingol Basin, Research on Grassland Ecosystem 1988,3, 84-183.
[20] Feng, X.; Zhao, Y. Grazing intensity monitoring in Northern China steppe: Integrating CENTURY model and MODIS data. Ecological Indicators 2011, 11(1):175–182.
[21] Kadono, A.; Funakawa, S.; Kosaki, T. Factors controlling mineralization of soil organic matter in the Eurasian steppe. Soil Biology and Biochemistry 2008, 40(4), 947-955.
[22] Sulla-Menashe, D.; Friedl, M.; Krankina, O.; Baccini. A.; Woodcock, C.; Sibley, A.; Sun, G.; Kharuk, V.; Elsakov, V. Hierarchical mapping of Northern Eurasian land cover using MODIS data. Remote Sensing of Environment 2011, 115, 392–403.
[23] Xie, Y.; Sha, Z.; Yu, M.; Bai, Y.; Zhang, L. A comparison of two models with Landsat data for estimating above ground grassland biomass in Inner Mongolia, China. Ecological Modelling 2009, 220(15), 1810-1818.
[24] Englhart, S.; Keuck, V.; Siegert, F. Modeling Aboveground Biomass in Tropical Forests Using Multi-Frequency SAR Data—A Comparison of Methods. IEEE J. Sel. Top. Appl. Earth Observations Remote Sensing 2012, 5(1), 298-306.
[25] Gleason, C. J.; Im, J. Forest biomass estimation from airborne LiDAR data using machine learning approaches. Remote Sensing of Environment 2012, 125, 80-91.
[26] Li, F.; Zeng, Y.; Luo, J.; Ma, R.; Wu, B.. Modeling grassland aboveground biomass using a pure vegetation index. Ecological Indicators 2015, 62, 279-288.
[27] Gao, J.; Chen, Y.; Lü, S.; Feng, C.; Chang, X.; Ye, S.; Liu, J. A ground spectral model for estimating biomass at the peak of the growing season in Hulunbeier grassland, Inner Mongolia, China. International Journal of Remote Sensing 2012, 33(13), 4029-4043.
[28] Maire, G. L.; Marsden, C.; Nouvellon, Y.; Grinand, C.; Hakamada, R.; Stape, J.; Laclau, J. MODIS NDVI time-series allow the monitoring of Eucalyptus plantation biomass. Remote Sensing of Environment 2011, 115(10), 2613-2625.
[29] Mäkelä, E.; Pekkarinen, A. Estimation of forest stand volumes by Landsat TM imagery and stand-level field-inventory data. Forest Ecology and Management 2004, 196, 245–255.
[30] Liang, D.; Zuo, Y.; Huang, L.; Zhao, J.; Teng, L.; Yang, F. Evaluation of the Consistency of MODIS Land Cover Product (MCD12Q1) Based on Chinese 30 m GlobeLand30 Datasets: A Case Study in Anhui Province, China. ISPRS Int. J. Geo-Inf. 2015, 4, 2519-2541.
[31] Ogay, R.; Barbeta, A.; Başnou, C.; Peñuelas, J. Satellite data as indicators of tree biomass growth and forest dieback in a Mediterranean holm oak forest Annals of Forest Sci.2015, 72(1), 135-144.
[32] Sha, Z.; Brown, D.; Xie, Y.; Welsh, B. Discriminating stocking rates in a typical grassland using in situ spectral reflectance data, Proceedings of the Earth Observation and Remote Sensing Applications, Shanghai, China, 2012/6/12-2012/6/13.
[33] Yan, Y.; Wang, S.; Chen, J. Spatial patterns of scale effect on specific sediment yield in the Yangtze River basin. Geomorphology 2011, 130(1-2), 29-39.
[34] Bradley, B.; Jacob, R. W.; Hermance, J. F.; Mustard, J. curve fitting procedure to derive inter-annual phenologies from time series of noisy satellite NDVI data. Remote Sensing of Environment 2007, 106(2), 137–145.

Zongyao Sha received degree in Photogrammetry & Remote Sensing from Wuhan University. He is Professor of GIS and Remote Sensing working at the department of Spatial Information & Digital Engineering, Wuhan University. Dr. Sha is interested in geospatial modeling, and classification algorithms and applications of remote sensing imagery. Particular focus is on studies of grassland ecology through integrated application of remote sensing technology and GIS and spatial data mining for ecosystems. He has been serving as PI of China's key research projects from National Science Foundation of China, Supporting Plan Program of Science and Technology, and Strategic Priority Research Program. Dr. Sha has published more than 40 peer-reviewed papers, including International Journal of Remote Sensing, ISPRS Journal of Photogrammetry and Remote Sensing, Remote Sensing Letters, etc, and is also author of 2 books.

Chunfang Wang got her Ph.D from the Chinese Academy of Sciences in

2006. Her priority research is in agriculture. She has published about 20 peer-reviewed papers.

TABLE 1. AG-BIOMASS INVERSION FROM GVIS BY DIFFERENT FUNCTIONS (N=310)

Scale	Model type	MODIS EVI		MODIS NDVI		SPOT-VGT NDVI		AVHRR NDVI	
		Function	R^2	Function	R^2	Function	R^2	Function	R^2
8km × 8km	Linear	$28.83+411.03x$	0.502	$31.89+243.11x$	0.539	$4.15+250.75x$	0.458	$33.03+208.47x$	0.456
	Quadratic	$-34.55+888.75x-828.66x^2$	0.523	$-2.94+412.08x-184.99x^2$	0.547	$-48.93+467.36x-206.77x^2$	0.464	$2.14+336.72x-121.84x^2$	0.461
	Power	$412.52x^{0.84}$	0.588	$258.34x^{0.77}$	0.616	$246.42x^{0.96}$	0.544	$228.29x^{0.76}$	0.515
	Exponential	$57.66e^{3.07x}$	0.542	$58.68e^{1.83x}$	0.590	$46.03e^{1.94x}$	0.534	$59.14e^{1.57x}$	0.500
4.5km × 4.5km	Linear	$18.67+444.26x$	0.696	$19.47+267.96x$	0.743	$-9.23+275.70x$	0.617		
	Quadratic	$-8.90+654.83x-366.58x^2$	0.701	$24.23+243.89x+26.77x^2$	0.743	$47.47+36.91x+233.36x^2$	0.626		
	Power	$434.08x^{0.88}$	0.725	$269.26x^{0.82}$	0.763	$253.99x^{1.00}$	0.633		
	Exponential	$53.41e^{3.32x}$	0.691	$53.18e^{2.03x}$	0.754	$41.66e^{2.13x}$	0.657		
1km × 1km	Linear	$20.27+437.71x$	0.673	$20.08+266.79x$	0.725	$-7.21+272.63x$	0.609		
	Quadratic	$-9.54+661.41x-384.19x^2$	0.680	$26.14+237.03x+32.84x^2$	0.725	$53.01+18.83x+248.38x^2$	0.618		
	Power	$425.20x^{0.87}$	0.695	$267.58x^{0.82}$	0.737	$252.62x^{0.99}$	0.637		
	Exponential	$54.79e^{3.23x}$	0.666	$54.15e^{1.99x}$	0.733	$42.56e^{2.10x}$	0.657		

All inversion models are significant at $p<0.0$

TABLE 2. MODEL VALIDATING USING SAMPLED DATA (N=151)

Scale	Model type	MODIS EVI		MODIS NDVI		SPOT-VGT NDVI		AVHRR NDVI	
		RMSE	RE (%)	RMSE	RE (%)	RMSE	RE (%)	RMSE	RE (%)
8km × 8km	Linear	33.16	17.70	31.92	16.46	34.65	18.34	34.66	18.02
	Quadratic	32.48	17.30	31.68	16.35	34.44	18.91	34.51	18.24
	Power	33.16	16.61	31.94	15.78	34.83	17.95	34.81	17.69
	Exponential	35.04	17.72	33.13	16.34	35.79	17.60	35.64	17.85
4.5km × 4.5km	Linear	25.02	13.83	22.95	12.17	27.97	16.16		
	Quadratic	24.78	13.86	22.94	12.12	27.62	15.31		
	Power	25.01	13.61	23.13	12.19	28.26	15.88		
	Exponential	27.50	14.34	23.74	12.26	27.86	14.98		
1km × 1km	Linear	25.71	14.66	23.60	12.70	28.14	16.12		
	Quadratic	25.44	14.67	23.59	12.66	27.77	15.34		
	Power	25.79	14.34	23.86	12.72	28.44	15.82		
	Exponential	28.39	15.24	24.34	12.79	27.94	15.00		

https://doi.org/10.17758/EAP.IAE0517312